*J. Synchrotron Rad.* (1999). **6**, 1076–1085

# ROBL – a CRG beamline for radiochemistry and materials research at the ESRF

**W. Matz,* N. Schell, G. Bernhard, F. Prokert, T. Reich, J. Claußner, W. Oehme, R. Schlenk, S. Dienel, H. Funke, F. Eichhorn, M. Betzl, D. Pröhl, U. Strauch, G. Hüttig, H. Krug, W. Neumann, V. Brendler, P. Reichel, M. A. Denecke and H. Nitsche**

*Forschungszentrum Rossendorf, Postfach 51 01 19, D-01314 Dresden, Germany. E-mail: w.matz@fz-rossendorf.de*

(*Received 19 March 1999; accepted 4 August 1999*)

The paper describes the Rossendorf beamline (ROBL) built by the Forschungszentrum Rossendorf at the ESRF. ROBL comprises two different and independently operating experimental stations: a radiochemistry laboratory for X-ray absorption spectroscopy of non-sealed radioactive samples and a general purpose materials research station for X-ray diffraction and reflectometry mainly of thin films and interfaces modified by ion beam techniques.

**Keywords: beamlines; EXAFS; XANES; radiochemistry laboratory; radionuclides; X-ray diffraction and reflectometry; thin films; interfaces; melts.**

## 1. Introduction

The Rossendorf beamline (ROBL) is a collaborating research group (CRG) beamline at the European Synchrotron Radiation Facility (ESRF). ROBL has been designed for performing experiments on two different experimental stations located in lead shielded hutches: a radiochemistry hutch (RCH) and a materials research hutch (MRH). X-ray absorption spectroscopy and X-ray diffraction and reflectometry are the main experimental techniques used in the RCH and MRH, respectively. Both end-stations operate alternatively.

The beamline was built and is operated by the Forschungszentrum Rossendorf (FZR) located near Dresden. Most of the beam time is used by the FZR for in-house research devoted to:

(i) Radioecological research as scientific background for risk assessment and development of remediation strategies for areas contaminated by radionuclides; determination of the chemical speciation of radionuclides interacting with geological material, natural and anthropogenic organics, and micro-organisms; study of the influence of these interactions on radionuclide migration and retardation in the environment.

(ii) Structural identification and characterization (including texture) of modifications of surfaces and interfaces produced by ion beam techniques for applications as hard covers, sensors or in semiconductor technology; study

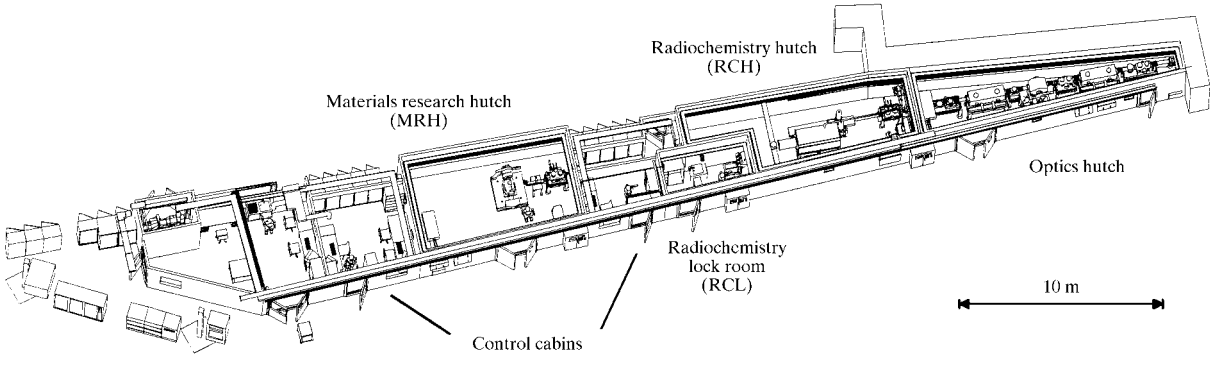


**Figure 1**
General layout of ROBL. The X-ray optics in the first hutch delivers monochromatic radiation either to the radiochemistry or to the materials research hutches. A total of three cabins are available for beamline and experiments control as well as for minor (non-radioactive) sample preparation and maintenance work.

of interfaces in thin films and nanometer-multilayers; structural investigations of melts and amorphous solids.

The beamline is also available to outside users to perform experiments either in collaboration with the FZR or by submitting a proposal to the ESRF: one-third of the ROBL beam time will be allocated by the ESRF for peer-reviewed experiments.

This paper describes the beamline design and its technical specifications as well as the standard experimental equipment of both experimental stations.

## 2. Beamline optics

The beamline is located at the bending-magnet port BM20 of the ESRF. The overall layout of ROBL is shown in Fig. 1. The beamline optics uses horizontally a fan of 2.8 mrad of synchrotron radiation from the hard edge of the ESRF bending magnet (0.8 T range, critical energy 19.6 keV) (ESRF, 1993). The layout of the optics is sketched in Fig. 2. The main elements are a fixed-exit double-crystal monochromator located between two mirrors. The beamline is designed for an energy range from 5 to 35 keV. The lower energy limit is given essentially by the mandatory Be windows. The upper energy limit was chosen to allow X-ray absorption spectroscopy (XAS) experiments on all chemical elements from Ti onward, since at least one absorption edge is in the energy range 5–35 keV.

### 2.1. *X-ray mirrors*

The two mirrors, with the same grazing angle, suppress the higher-order harmonics in the monochromatic beam, reduce the heat load on the monochromator, and provide a parallel or vertically focused beam at the experimental stations at a fixed height, as dictated by safety requirements for the radiochemistry hutch (see §3.3).

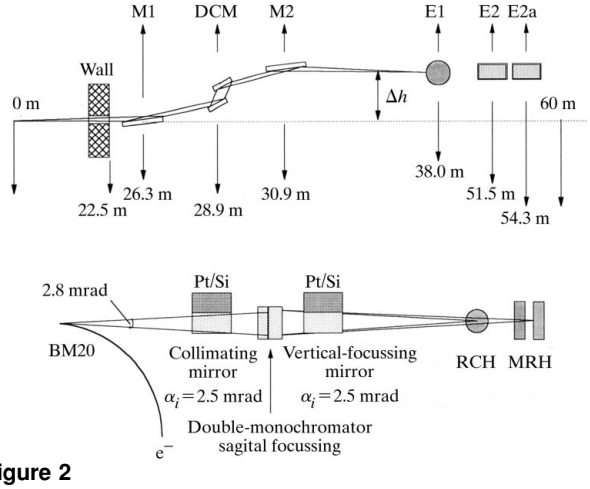


**Figure 2**
Scheme of the X-ray optics of ROBL. A mirror–double-crystal monochromator–mirror arrangement selects a monochromatic beam for the two experimental end-stations. M1 – first mirror; DCM – double-crystal monochromator; M2 – second mirror; E1 – radiochemical experiment; E2 – goniometer; E2a – third experiment.

With a fixed angle of incidence of 2.5 mrad and a length of 1200 mm, the first mirror intercepts only 3 mm of the vertical beam divergence corresponding to about 55% at 12 keV and about 72% at 25 keV of the incoming photons. The calculated spectral flux for the two cases is shown in Fig. 3. The intensity decrease below 10 keV is due to the absorption of the beryllium windows. For the main applications of ROBL the most important energy regions are below 10 keV and between 16 and 22 keV. To avoid disturbances in these energy regions, resulting from absorption edges of the mirror coatings, the mirror substrates were coated with two parallel stripes of silicon and platinum that are used alternatively. The harmonic suppression is better than $8 \times 10^{-4}$ for all energies when using the silicon stripes. For the platinum stripes it is of the same order of magnitude for energies above 13.5 keV.

The X-ray mirrors including cooling and bending mechanisms were purchased (Zeiss). The first mirror is made of a single Si crystal which is water-cooled from the side (Pauschinger *et al.*, 1995). The second mirror uses a Zerodur substrate without cooling. Both mirrors are equipped with pneumatic benders. The first is bent with a radius of 20.8 km to collimate the incident radiation onto the first monochromator crystal. The second, with an adjustable bending radius down to 8 km, focuses the beam vertically to the two experimental end-stations.

### 2.2. *Double-crystal monochromator*

The double-crystal monochromator (DCM) provides a fixed-exit beam with a vertical offset of 18 mm. It operates with either Si(111) or Si(311) crystal sets. The mechanical

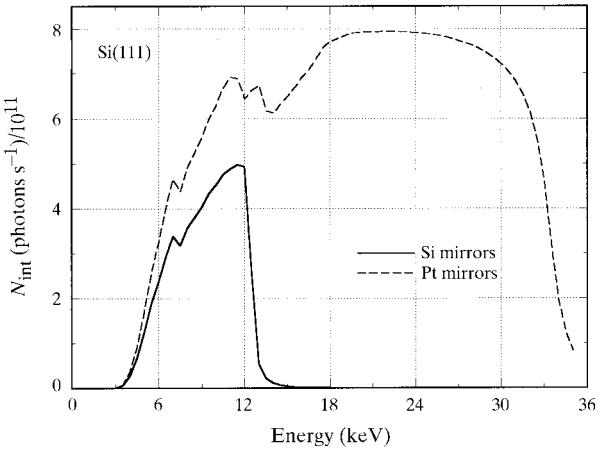


**Figure 3**
Calculated flux of focused radiation with silicon- and platinum-coated mirrors and Si(111) crystals in the double-crystal monochromator obtained using the *SHADOW* code (Matz *et al.*, 1996; Lai & Cerrina, 1986). The attenuation from beryllium windows of total thickness 1.5 mm is included. The dip at around 7 keV results from the experimental absorption curve of the technical Be used as window material. The maximum energy of 35 keV can be realized only with Si(311) monochromator crystals. Geometrical constraints of the DCM design limit the accessible energy range for Si(111) crystals to about 25 keV.

construction allows 25 keV to be reached using Si(111) crystals, and 35 keV using Si(311) crystals. The design is mainly a commercial one (Oxford Instruments, ATG): the axis of a high-precision rotation table is fed into a vacuum vessel. A crystal cage mounted on this axis carries both crystals. The first crystal is mounted with the rotation axis on the reflecting surface. The second crystal can be moved relative to the first one, parallel and perpendicular to the beam direction. The combined motion of both drives realizes a fixed-exit beam. The first crystal position can be adjusted only manually, while all movements of the second crystal are motorized and remote controlled, allowing both alignment with the beam and a fine tuning by piezoelectric translators.

The first crystal is water cooled. The cooling water is supplied by individual jets directed into slots machined in the back of the crystal. Bridges between the cavities provide stability to the reflecting crystal surface. The second crystal will be equipped with a bender (ESRF design) for sagittal focusing; in the beginning it will be available only for Si(311).

For quick-EXAFS, a pseudo channel-cut mode of the monochromator is possible by keeping fixed the position of the second crystal relative to the first one. In this mode only the Bragg angle of the DCM is changed during a scan; for energies above 14 keV the beam height variation during a 500 eV wide scan is less than 0.6 mm.

A feedback system is installed which compensates intensity modulation during XAS scans by fine tuning the orientation of the second crystal on the base of a signal coming from a monitor in front of the sample.

The overall energy resolution of ROBL is shown in Fig. 4. This resolution allows the study of the near-edge structure at all absorption edges within the accessible energy range with a resolution better than the core-hole width.

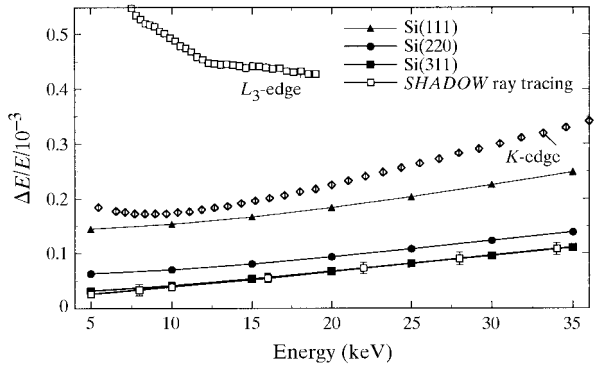


**Figure 4**
Calculated energy resolution of the double-crystal monochromator with silicon crystals and parallel incident beam. For comparison the natural line widths of the absorption edges of the elements are shown. Besides the analytically calculated values, results obtained using the *SHADOW* code are included for Si(311).

**Table 1**
Characteristic data of the monochromatic synchrotron beam.

| | |
|---|---|
| Energy range | 5–35 keV |
| Energy range with Si mirrors | 5–12 keV |
| Energy resolution with Si(111) crystals | 1.5–2.5 × $10^{-4}$ |
| Energy resolution with Si(311) crystals | 0.5–1.0 × $10^{-4}$ |
| Integrated flux for focused beam (calculated) | 6 × $10^{11}$ photons $s^{-1}$ at 20 keV, 200 mA |
| Standard beam size | 20 mm (w) × 3 mm (h) |
| Focused beam size | ≤0.5 mm × 0.5 mm |

### 2.3. *Other optical elements*

In addition to the mirrors and the monochromator, the optics contains various slit units, filters and beam-position monitors. The slit units have independently moveable blades (tungsten carbide), with an accuracy in the horizontal and in parallelism better than 10 μm. The filter unit has six absorber foils to attenuate the white beam. The beam-position monitors consist of scanning wires.

The motions of nearly all optical components are motorized, mostly with stepper motors, controlled by a UNIX workstation-based system. Many standard ESRF software applications are used in the control programs, which utilize the *SPEC* code package (Swislow, 1996).

The control system also includes interlock components for the vacuum, beam shutters and the cooling of components exposed to the white beam. Fig. 5 shows the arrangement of the beamline optics in detail. The characteristics of the monochromatic beam are summarized in Table 1.

## 3. Radiochemistry end-station

The radiochemistry end-station is designed for studying radionuclides of environmental importance such as Tc, U, Th, Np, Pu and Am. X-ray absorption spectroscopy is a powerful technique for obtaining information on the molecular and electronic structure of these radionuclides in solids and liquids. It is an element-specific method and provides information about the oxidation state as well as the bond lengths and numbers of neighbouring atoms in the first, second and even third coordination shell of the absorber. Such knowledge is essential for understanding complexation and speciation of radionuclides and also absorption processes from solutions. Actinides are known to exist in many oxidation states which are difficult to determine by chemical or optical methods. In contrast, XAS can distinguish the oxidation state from the shift of the absorption edge, also providing information if different states are present in one sample. For example, the actinide oxidation states An(V) and An(VI) are often distinguishable from An(III) and An(IV) due to the presence of a multiple-scattering resonance in the An $L_3$-edge XANES of the trans-dioxo cations $AnO_2^+$ and $AnO_2^{2+}$. Another advantage of XAS for radiochemical investigations is the possibility of using solid or liquid samples as well as very dilute ones (micro-mol region). Such aspects were the

motivation for setting up the radiochemical part of ROBL in relation to the radioecological research program at FZR (Nitsche *et al.*, 1999).

### 3.1. *Synchrotron radiation beamlines for studying radioactive materials*

During the last five years the number of experiments with radioactive materials performed worldwide at synchrotron radiation beamlines increased significantly. This increase was possible due to two achievements: (i) implementation of special procedures for experiments with radioactive materials at existing general-user beamlines, and (ii) construction of beamlines dedicated to the study of radioactive samples.

X-ray absorption fine structure (XAFS) measurements of samples with natural uranium have been performed at several synchrotron storage rings in Europe, USA and Japan (Petiau *et al.*, 1986; Kalkowski, Kaindl, Brewer & Krone, 1987; Dent *et al.*, 1992; Chisholm-Brause *et al.*, 1994; Hudson *et al.*, 1995; Allen, Shuh *et al.*, 1996; Giaquinta *et al.*, 1997; Denecke *et al.*, 1997; Den Auwer *et al.*, 1997; Yaita *et al.*, 1998). However, experiments with transuranics have been very limited in number (Kalkowski, Kaindl, Bertram *et al.*, 1987; Petit-Maire *et al.*, 1989; Combes *et al.*, 1992). In 1993 a US Department of Energy review established the fundamental basis of experimental and safety procedures for transuranic experiments at the Stanford Synchrotron Radiation Laboratory (SSRL), which enabled several EXAFS studies of solutions and solids containing Np and Pu (Allen, Veirs *et al.*, 1996; Allen *et al.*, 1997; Clark *et al.*, 1997, 1998; Conradson, 1998; Den Auwer *et al.*, 1999). At SSRL the maximum allowed quantity of $^{237}$Np in the experimental X-ray hutch at any one time must be less than 50 μCi. The total amount of Np material that can be shipped to and be present at SSRL at any one time must be less than 500 mg (325.5 μCi) to ensure that the Stanford Linear Accelerator Center (SLAC) remains a low-hazard non-nuclear facility (Allen *et al.*, 1999).

**Table 2**
List of radioactive elements which can be investigated at ROBL, and the maximum amount of material to remain below the activity limit of 5 mCi.

| Isotope | Half-life (years) | Amount (g) |
|---|---|---|
| Np 237 | $2.1 \times 10^{6}$ | 6.97 |
| Am 241 | 433 | $1.4 \times 10^{-3}$ |
| Am 243 | 7370 | 0.025 |
| Po 208 | 2.9 | $8 \times 10^{-6}$ |
| Po 209 | 103 | $3.01 \times 10^{-4}$ |
| Pa 231 | $3.28 \times 10^{4}$ | 0.106 |
| Pu 239 | $2.4 \times 10^{4}$ | 0.08 |
| Pu 242 | $3.75 \times 10^{5}$ | 1.27 |
| Ra 226 | 1600 | 0.005 |
| Tc 99 | $2.1 \times 10^{5}$ | 29.1 |
| U natural | $4.47 \times 10^{9}$ | 1000 |
| Th natural | $1.4 \times 10^{10}$ | 1000 |

Dedicated beamlines for the study of radioactive materials have become operational in Japan at the Photon Factory (PF) and SPring-8. The PF beamline consists of two branches covering the energy ranges 1.8–6 keV and 4–20 keV (Konishi *et al.*, 1996). The experimental station in the hard X-ray range is dedicated to diffractometry and XAFS studies. By a special monochromator adjustment the energy range for XAFS experiments can be extended to 24 keV. In the soft X-ray range the experimental possibilities to study radioactive materials have been further improved by the construction of an end-station at SPring-8 which provides linearly or circularly polarized light in the energy range 0.28–1.5 keV (Yokoya *et al.*, 1998).

The ROBL-CRG obtained a license from the French authorities to perform XAFS experiments with the isotopes listed in Table 2. Under this license the maximum allowed activity at any given time present at ROBL is 185 MBq (5 mCi). These elements emit mostly $\alpha$ and $\beta$ particles and only weak $\gamma$-radiation. Therefore, the heart of the radiochemistry end-station is a glove box without additional lead shielding. To ensure a safe handling of the radionuclides the entire experimental station is built as a radiochemistry

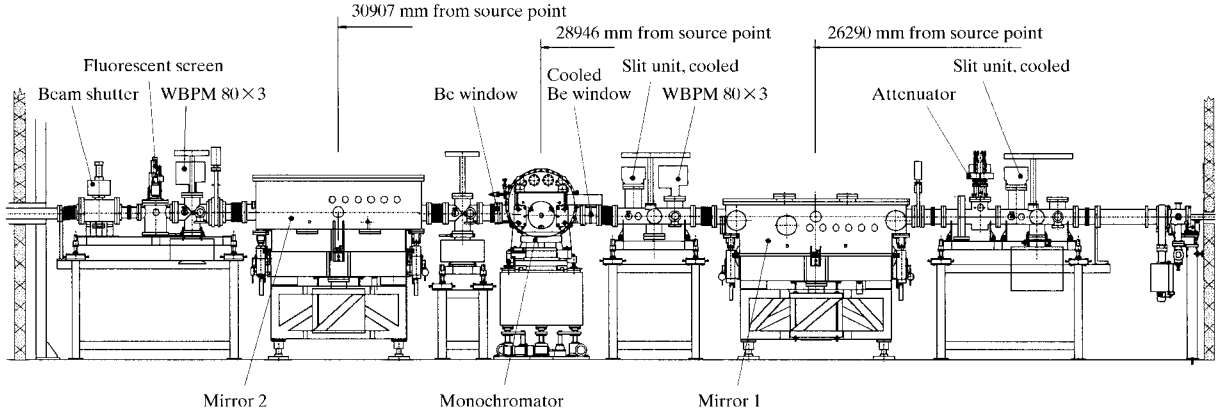


**Figure 5**
Technical drawing of all components of the beamline optics. The distances of the double-crystal monochromator and the mirrors from the source point are indicated. WBPM – wire beam-position monitor.

laboratory according to legal safety requirements. The advantages of the ROBL radiochemistry station when compared with the other synchrotron radiation beamlines are manyfold: (i) the maximum allowed amount of radioactive material is 5 mCi which is higher than at most other synchrotron light sources, (ii) it is the only dedicated end-station for XAFS experiments of actinides in Europe. In addition, to our knowledge, ROBL is the only XAFS station in the world where it is possible to manipulate the chemical and physical properties of the sample in a glove box on-site and during the experiment at a third-generation high-energy synchrotron radiation source.

### 3.2. *Experimental set-up for XAFS*

The XAFS spectra can be measured both in transmission and fluorescence modes. For transmission mode the sample is placed perpendicular to the photon beam between two ionization chambers (OHYO KOKEN KOGYO). In fluorescence mode the sample is inclined by 45° with respect to the beam, and the fluorescence radiation is detected with Ge solid-state detectors (Lawrence Berkeley National Laboratory) positioned perpendicular to the beam. The radioactive samples are positioned inside the glove box equipped with 125 μm-thick kapton (polyimide) windows which are transparent to hard X-rays. All detectors, *e.g.* gas ionization chambers and fluorescence detectors, are mounted on an optical bench outside the glove box. This arrangement allows a direct and easy access to the detectors and avoids bringing signal cables, gas and power supply lines into the glove box. In addition, even in the unlikely case of a contamination inside the glove box, the detectors will not be affected.

Inside the glove box it is possible to use sample holders at different positions. Two, marked (*a*) and (*b*), are indicated in the schematic glove box layout of Fig. 6. At position (*a*) a larger space is available so it is possible to mount either an automatic sample holder, which provides room for up to eight solid or liquid samples, or a closed-cycle He cryostat. The samples in position (*a*) can be measured both in transmission and fluorescence modes. For measurements on very dilute samples a special single-sample holder can be placed at position (*a*). The rotating arm of this positioning system moves the sample to position (*b*), between two kapton windows and rotates it at 45° with respect to the beam: two Ge solid-state detectors record simultaneously the fluorescence signals.

Since the samples are safely contained in the glove box, it is possible to change some of the sample conditions during the experiment. With the closed-cycle He cryostat (custom designed from Oxford Instruments) the sample temperature can be varied between 10 K and 295 K. It is also possible to modify the chemical conditions of liquid samples just before or during the XAFS measurements by adding non-radioactive substances like acids, bases or complexing agents.

The glove box is mounted on a support frame which allows movement of the glove box in the horizontal direction out of the beam leaving the position of the optical bench and of the detectors unchanged. Thus, non-radioactive samples can be easily measured outside the glove box by mounting them on the optical bench between the first and second ionization chambers. For energy-calibration purpose a non-radioactive reference sample can be placed between the second and third gas ionization chambers. The reference sample is inside a fluorescence X-ray ion chamber detector (Lytle detector; EXAFS Company) which offers the possibility of recording the XAFS also in fluorescence mode.

When measurements take place downstream in the MRH, the box and the optical bench are moved out of the beam horizontally and vertically, respectively, and the beam path in the RCH is closed by a vacuum pipe to reduce the loss of beam intensity.

### 3.3. *Safety concept for radioactive work*

In order to guarantee a safe operation of the experiments with radioactive samples a number of safety installations were made to monitor the actual status. Basically a

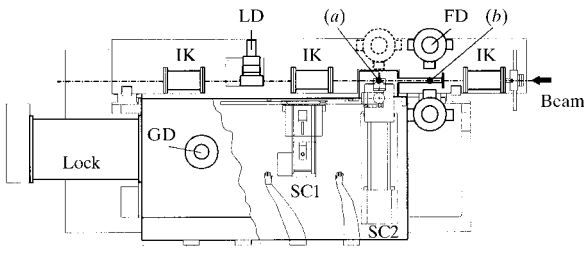


**Figure 6**
Principal layout of the glove box. (*a*) Standard sample position for XAFS experiments; (*b*) sample position for fluorescence radiation detection from dilute liquid samples. The ionization chambers (IK) are mounted on an optical bench and can also be used for non-radioactive samples while the box is moved out of the beam. FD – fluorescence detector; LD – Lytle detector; GD – gamma detector for measurement of sample activity. SC1 and SC2 are sample changers 1 and 2, respectively.

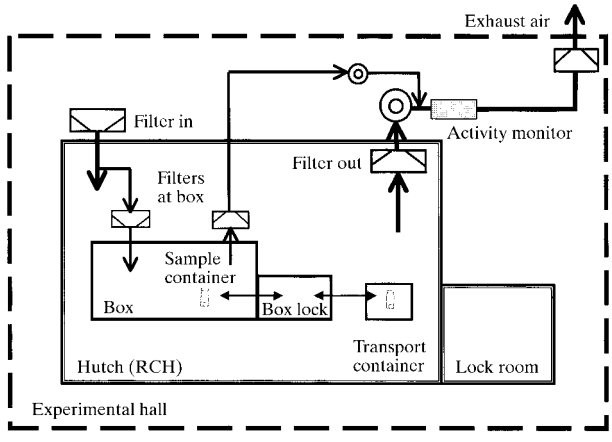


**Figure 7**
Scheme of the multibarrier concept for the safety system of the radiochemistry hutch of ROBL.

multibarrier concept is realized here, as usual for radiochemical work, whose concept is schematically shown in Fig. 7. The samples are enclosed in an X-ray transparent container serving as the first barrier. The sample container itself is either inside a multiwalled transport container or within the glove box. The glove box is the second barrier under experiment conditions. The glove box is located in the hutch which is a third barrier towards the experimental hall of the ESRF. Therefore, the radiochemistry hutch is equipped with a closed inner wall in addition to the lead wall for radiation shielding. It is made of steel panels, sealed by epoxy resin. The two functions so achieved are (i) a good air tightness of the hutch in order to allow for a pressure gradient to the hall, and (ii) to provide a smooth surface if decontamination is necessary. The condition of air tightness of the RCH requires that the incoming synchrotron radiation beam is always at the same height as achieved by ROBL optics. The floor has a highly resistant plastic covering. All equipment is mounted on plates. The interfaces between the floor covering and the walls, as well as the mounting plates, are sealed by epoxy resin.

The negative pressure gradient from hall to hutch and from hutch to glove box is established by a special air-ventilation system for the RCH, independent of all other systems both of ROBL and ESRF: it performs eight complete volume changes of air per hour. Separate ventilators for the glove box and the hutch exhaust air, each with high-absorption absolute aerosol filters, ensure an automatically regulated pressure difference of 200 Pa between the glove box and the hutch. The exhaust air will be controlled by a permanent monitoring system outside the RCH to be free from radiation background effects. Before the filtered and monitored exhaust air leaves the experimental hall over the roof, a final filter is inserted as a last barrier to the environment.

The personnel access to RCH is possible only through the lock room (RCL in Fig. 1), where a change of coats and shoes has to be performed. After leaving the RCH the users have to check themselves with the personnel monitor for possible contamination and to change clothing again.

The $\alpha/\beta$-activity, as well as the dose rate of the air inside the RCH, is permanently controlled by a moving filter aerosol monitor. All safety-related data are continuously collected in a signalization system, which optically and acoustically indicates all changes, failures and deviations from reference values within the safety system. In case of an emergency in the RCH the signalization system will cause the closing of the beam shutter and of the vacuum valves *via* the ESRF interlock system.

For the identification and documentation of the different samples a $\gamma$-spectrometer is mounted on the floor inside the glove box (GD in Fig. 6). A hand–foot monitor in the lock room, movable $\alpha/\beta$ and dose-rate counters and a fixed $\alpha/\beta$ measuring station complete the safety equipment of the RCH.

The preparation of radioactive samples is not possible at the ESRF. Samples will be transported to the experimental end-station in certified 'transport containers' made of steel. They contain the 'working container' equipped with 1 cm lead walls absorbing all radioactive radiation up to a limit of 5 $\mu$Sv h$^{-1}$. This working container will be opened only in the glove box where the polyethylene 'sample container' will be removed.

### 3.4. *Performance tests by XAFS spectroscopy*

To check the energy calibration of the Si(111) double-crystal monochromator the X-ray absorption near-edge structure (XANES) spectra of several metal foils in the energy range 5–30 keV were measured in transmission mode. The absorption edges values found for Ti, Cr, Co, Zn, Zr, Nb and Sb foils were compared with the values given by Kraft *et al.* (1996). The data evaluation showed that the standard deviation of the Bragg angle was less than 0.002° in the entire energy range indicating an excellent linearity of the monochromator mechanics. Fig. 8 displays single sweeps of *K*-edge XANES spectra of three representative elements. The features of the Ti and Zr *K*-edges are well resolved, as expected from the high resolution of the beamline, that is lower than the material core-hole lifetime.

The performance of the whole beamline optics and detector system is also demonstrated by the high quality and extended *k*-range of the Tc *K*-edge $k^3$-weighted extended X-ray absorption fine-structure (EXAFS) spectrum shown in Fig. 9. This transmission spectrum of a 0.1 *M* Tc(VII) solution is the result of a single energy sweep. At

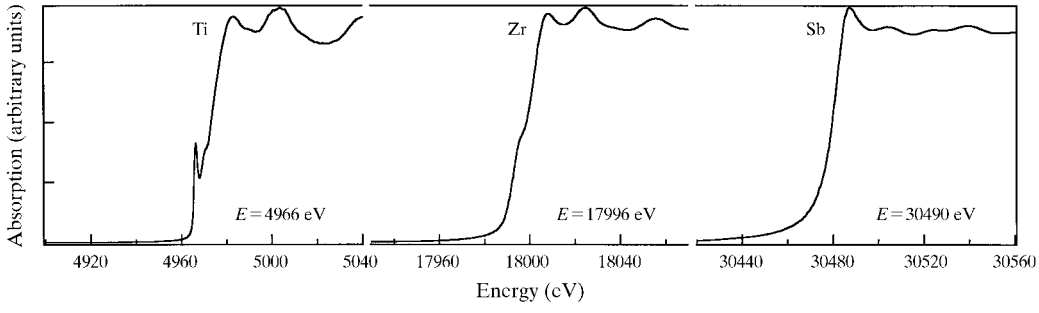


**Figure 8**
*K*-edge XANES spectra of metallic Ti, Zr and Sb. The energy scale was calibrated using the edge energies given by Kraft *et al.* (1996). The natural line widths of the Ti, Zr and Sb *K* shells are 0.94, 3.84 and 9.16 eV, respectively (Krause & Oliver, 1979).

the beginning of the EXAFS region the counting time per point was 1 s. The measuring time was continuously increased with $k$ and reached 20 s point$^{-1}$ at $k$ = 20 Å$^{-1}$.

## 4. Materials research end-station

The materials research end-station is mainly devoted to structural studies of solids and melts by diffraction and reflectometry. The field of interest for the in-house research are crystalline phases and structural changes in thin near-surface regions of solids. Mainly samples produced or modified by ion beam techniques will be investigated, but the diffractometer is versatile enough to allow for a wider range of applications than thin-film studies. A special design was made for the diffraction on melts with free surfaces.

### 4.1. *Goniometer*

The goniometer (Fig. 10) in the MRH is a six-circle goniometer built from standard components (Huber). The arrangement of two parallel circles each with horizontal and vertical axes, respectively, allows experiments in both scattering planes. The sample position can be equipped with an $x$-$y$-$z$ slide or, alternatively, with special sample environment chambers which are mounted directly on the $\varphi$-circle. The layout is designed for a load up to 15 kg at the sample position and the $\chi$-circle has an inner diameter of 400 mm so that even huge and heavy chambers (*e.g.* a high-temperature chamber) can be used without difficulties. All axes are equipped with stepping motors and gear boxes which allow a minimum angular step of 0.0001°. The $z$-translation of the $x$-$y$-$z$ slide has a step width of 1 µm while the two other translations have step widths of 10 µm. Additionally, sample holders for single-crystal samples and capillary sample containers are available.

The goniometer is fully computer controlled by a workstation and the programs are based on the *SPEC* code (Swislow, 1996).

Different detection systems can be mounted at the detector arm. As standard, a high-load high-linearity scintillation detector is used (BEDE). In front of the detector, interchangeable fixed single or Soller slits can be mounted. Other detection systems are a two-dimensional CCD

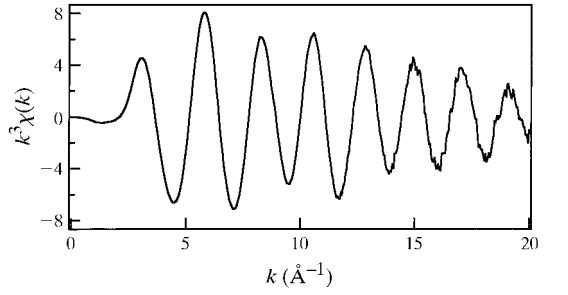


**Figure 9**
Single sweep of the Tc $K$-edge $k^3$-weighted EXAFS spectrum of a 0.1 $M$ pertechnetate, $TcO_4^-$, solution.

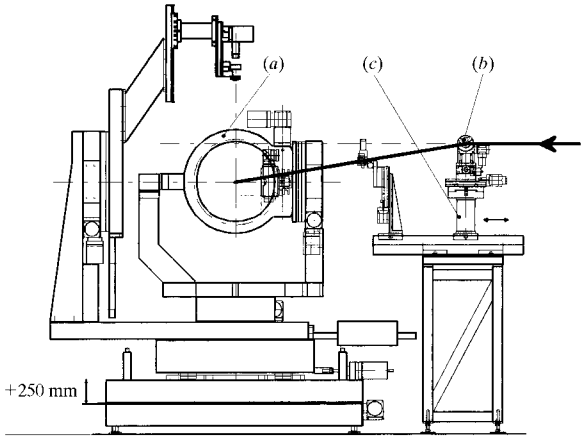


**Figure 10**
Scheme of the goniometer (*a*) in the materials research end-station and of the deflector unit (*b*) for the study of melts with free surfaces. The small goniometer head with the deflecting multilayer mirror (*b*) can be positioned at different distances to the sample by a translation slide (*c*).

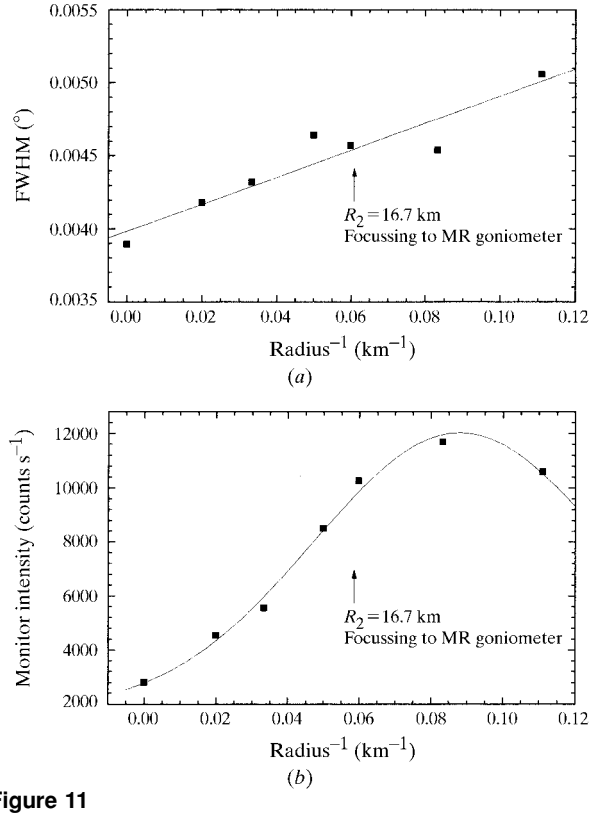


**Figure 11**
(*a*) Divergence of the beam at the MRH goniometer measured by the FWHM of the rocking curve of the Si(400) single-crystal reflection as a function of the bending of mirror M2 (bending radius of mirror M1 = 20.93 km, wavelength λ = 0.10008 nm). The sample was Si⟨100⟩ implanted with 5 × 10$^{15}$ C$^+$ (195 keV) cm$^{-2}$ at 773 K (non-ideal crystal). (*b*) Intensity variation of the incident beam at the MRH goniometer position as a function of the bending of mirror M2 under the same conditions.

camera (SMART) or an energy-dispersive pin photodiode. Optionally, a secondary monochromator unit (crystal analyser) may be mounted in front of the detector.

### 4.2. *Resolution for X-ray diffraction*

The resolution of a diffraction experiment depends not only on the energy resolution of the monochromator but also on the beam divergence. The experimentally achievable resolution was measured using silicon single crystals and powders. At present, radiation with the natural horizontal divergence of the synchrotron radiation beam from the source is used since the sagittal focusing option at the monochromator is not yet installed. The vertical divergence is reduced by the first collimating mirror.

Using the Si(111) monochromator and the Si mirrors at 12 keV and a vertically parallel beam, the FWHM of an Si(004) single-crystal reflection was measured to be $\Delta\theta = 0.003^\circ$ (10 arcsec). This corresponds approximately to a resolution $\Delta d/d = 1.3 \times 10^{-4}$. Vertical focusing with the second mirror raises the FWHM up to $0.0051^\circ$ but increases the incident radiation intensity significantly, as shown in Fig. 11. It follows from these results that ROBL's optics allows optimizing the intensity by vertical focusing without significant loss in resolution for polycrystal diffraction experiments.

A comparison of powder with single-crystal results for the Si(111) reflection at the energy of Cu $K\alpha$ radiation is shown in Fig. 12. For powder diffraction the instrumental contribution to the intrinsic FWHM of the Bragg peak was estimated. The angular resolution in the case of the Si(111) sample is entirely determined by the convolution of the incident- and receiving-slit apertures. Since mirror M1 is used as a collimating mirror it transmits the source divergence of 11 µrad. The focusing mirror M2 contributes about 150 µrad, so that the incident aperture amounts 151 µrad. Using a capillary of 0.4 mm diameter and a detector slit width of 0.22 mm in a distance of 0.5 m from the sample, one obtains for the receiving slit aperture 913 µrad. The latter part dominates the angular resolution (FWHM) for the Si(111) powder peak which amounts to about 925 µrad = $0.0530^\circ$.

The profile fitting of the measured Si(111) peak (line in Fig. 12) with a pseudo Voigt function [$F_{PsV} = \eta F_L + (1 - \eta)F_G$] gives a FWMH of $0.0528^\circ$ which agrees with the estimated value above. The very small $\eta$-parameter ($\eta = 0.0485$) indicates that the instrumentally determined Gaussian part dominates over the sample-broading effects expressed by the Lorentzian term.

To obtain the full possible resolution for powder diffraction (0.01–0.03°) it is possible to use a narrower receiving slit or a perfect crystal analyser.

Typical Si-powder resolution curves $\Delta d/d$ for different energies are given in Fig. 13. These data show that the materials research end-station is also suitable for high-resolution X-ray powder diffraction and for the study of line-broadening effects (Thiele *et al.*, 1999).

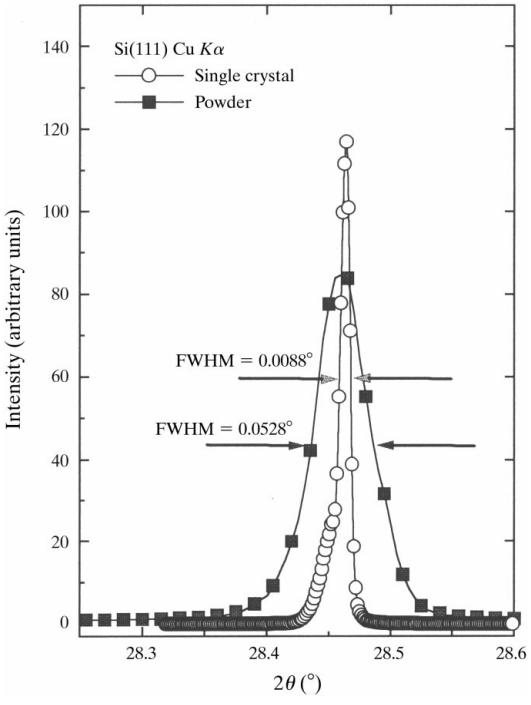


**Figure 12**
Comparison of the FWHM of the Si(111) reflection from a single crystal and a powder. The energy of the radiation was made equal to Cu $K\alpha$ radiation. Note that in contrast to Fig. 11 the full Bragg angle $2\theta$ is plotted. The wing at the low-angle side of the single-crystal peak results from deformations of the wafer due to ion implantation.

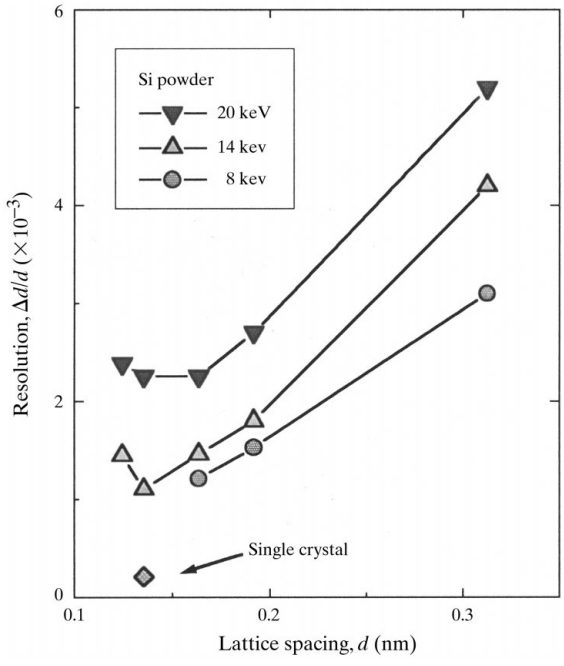


**Figure 13**
Experimental resolution $\Delta d/d$ obtained on silicon powder inside a glass capillary (diameter 0.4 mm; wall thickness 0.01 mm). For comparison the value from a single-crystal sample is indicated. The Si(111) monochromator crystals are used.

### 4.3. *Special set-up for the study of melts*

One of the scientific goals of ROBL is the study of melts (or more general liquids) with free surfaces by diffraction. This requires an incident beam inclined to the horizontal, to hit the horizontal surface of the melt. The additional demand to tune the energy in order to make use of anomalous scattering led to the installation of a deflection unit (*b*) as displayed in Fig. 10. A suitable multilayer mirror of $40 \times 100\ \mathrm{mm}^2$ is mounted on a circle with a horizontal rotation axis perpendicular to the incident beam and deflects the beam downwards. The deflecting multilayer mirror is made from $W/B_4C$ with a $2d$-value of 3 nm (Osmic); its reflecting efficiency is 50% at 8 keV. To ensure that the deflected beam is able to hit the sample, the goniometer has a motorized height adjustment. The sample position can be set 250 mm below the primary beam from the monochromator.

When changing the energy of the incident beam the deflection angle of the mirror and the height of the sample have to be changed. To avoid height adjustment of the huge diffractometer where the sample is mounted, the multilayer-mirror deflection unit is mounted on an additional translation stage (*c*). Thus, leaving the sample height fixed, the adjustment is performed by translation and rotation of the deflecting mirror alone, for an energy range of 5 keV when working at 10 keV and of 11 keV when working at 25 keV.

### 4.4. *Comparison with other beamlines*

The material research hutch (ROBL-MRH) opens additional possibilities in X-ray diffraction on polycrystals and liquids at the ESRF. The dedicated ESRF powder-diffraction beamline (BM16), as well as the powder-diffraction set-up of the Swiss–Norwegian beamline (BM1), are equipped with goniometers which are restricted to one scattering plane (Fitch, 1995, 1996; ESRF, 1997). ROBL-MRH offers horizontal and vertical scattering planes as well as off-plane diffraction possibilities. For powder or polycrystalline samples we provide the same diffraction resolution and nearly the same wavelength range as the mentioned beamlines.

Concerning the study of liquids with free surfaces, the ROBL-MRH set-up described in §4.3 is complementary to the BM32 set-up. The latter uses a silicon crystal in Laue geometry as beam deflector (Daillant *et al.*, 1996). This arrangement requires the movement of the goniometer in two directions to follow the Bragg cone of the radiation scattered from the deflector. The use of a multilayer as deflector at ROBL-MRH reduces the necessary movements of the goniometer to the up–down direction. Moreover, this design makes the arrangement of samples in chambers with small radiation windows easier.

## 5. Outlook

The ROBL beamline with both end-stations became fully operational in fall 1998. First experiments show a reliable performance of the entire beamline and its components. This CRG beamline adds new experimental possibilities to the ESRF. The radiochemistry end-station is the first dedicated set-up for XAFS studies of unsealed liquid radioactive samples at a modern synchrotron source. The materials research end-station allows diffraction in both scattering planes at a goniometer which can carry heavy sample chambers.

The authors acknowledge the continuous support by the directors of the FZR which makes the project possible, especially the first Scientific Director Professor W. Häfele. ROBL is financed by equal shares from the Saxonian Ministry of Science and Culture and the Federal Ministry of Research and Education *via* the budget of the FZR. Great support was given by many colleagues from the ESRF and the other CRG beamlines. We want to thank in particular I. Kilvington, P. Pattison, P. Berkvens, M. Belakhovsky, A. Fitch, E. Bräuer-Krisch, M. Hagelstein, D. Schmied and G. Peppelin.

## References

Allen, P. G., Bucher, J. J., Shuh, D. K., Edelstein, N. M. & Reich, T. (1997). *Inorg. Chem.* **36**, 4676–4683.
Allen, P. G., Shuh, D. K., Bucher, J. J. & Edelstein, N. M. (1999). *Speciation, Techniques and Facilities for Radioactive Materials at Synchrotron Light Source: Workshop Proceedings*, Grenoble, France, 4–6 October 1998, pp. 163–179. Paris: OECD/NEA.
Allen, P. G., Shuh, D. K., Bucher, J. J., Edelstein, N. M., Reich, T., Denecke, M. A. & Nitsche, H. (1996). *Inorg. Chem.* **35**, 784–787.
Allen, P. G., Veirs, D. K., Conradson, S. D., Smith, C. A. & Marsh, S. F. (1996). *Inorg. Chem.* **35**, 2841–2845.
Chisholm-Brause, C., Conradson, S. D., Buscher, C. T., Eller, P. G. & Morris, D. E. (1994). *Geochim. Cosmochim. Acta*, **58**, 3625–3631.
Clark, D. L., Conradson, S. D., Koegh, D. W., Palmer, P. D., Scott, B. L. & Tait, C. D. (1998). *Inorg. Chem.* **37**, 2893–2899.
Clark, D. L., Conradson, S. D., Neu, M. P., Palmer, P. D., Runde, W. & Tait, C. D. (1997). *J. Am. Chem. Soc.* **119**, 5259–5260.
Combes, J. M., Chisholm-Brause, C. J., Brown, G. E. Jr, Parks, G. A., Conradson, S. D., Eller, P. G., Triay, I. R., Hobart, D. E. & Meijer, A. (1992). *Environ. Sci. Technol.* **26**, 376–382.
Conradson, S. D. (1998). *Appl. Spectrosc.* **52**, A252–279.
Daillant, J., Quinn, K., Gourier, C. & Rieutord, F. (1996). *J. Chem. Soc. Faraday Trans.* **92**, 505–513.
Den Auwer, C., Madic, C., Berthet, J. C., Ephritikhine, M., Rehr, J. J. & Guillaumont, R. (1997). *Radiochim. Acta*, **76**, 211–218.
Den Auwer, C., Revel, R., Charbonnel, M. C., Presson, M. T., Conradson, S. D., Simoni, E., Le Du, J. F. & Madic, C. (1999). *J. Synchrotron Rad.* **6**, 101–104.
Denecke, M. A., Pompe, S., Reich, T., Moll, H., Bubner, M., Heize, K. H., Nicolai, R. & Nitsche, H. (1997). *Radiochim. Acta*, **79**, 151–159.
Dent, A. J., Ramsay, J. D. F. & Swanton, S. W. (1992). *J. Colloid Interface Sci.* **150**, 45–60.
ESRF (1993). *ESRF Beamline Handbook*, August 1993, pp. 9–10. Grenoble: ESRF.
ESRF (1997). *ESRF Beamline Handbook*, 4th ed., January 1997, pp. 25–29. Grenoble: ESRF.
Fitch, A. N. (1995). *Nucl. Instrum. Methods Phys. Res. B*, **97,** 63–69.

Fitch, A. N. (1996). *Mater. Sci. Forum*, **228–231**, 219–222.
Giaquinta, D. M., Soderholm, L., Yuchs, S. E. & Wasserman, S. R. (1997). *Radiochim. Acta*, **76**, 113–121.
Hudson, E. A., Rehr, J. J. & Bucher, J. J. (1995). *Phys. Rev. B*, **52**, 13815–13826.
Kalkowski, G., Kaindl, G., Bertram, S., Schmiester, G., Rebizant, J., Spirlet, J. C. & Vogt, O. (1987). *Solid State Commun.* **64**, 193–196.
Kalkowski, G., Kaindl, G., Brewer, W. D. & Krone, W. (1987). *Phys. Rev. B*, **35**, 2667–2677.
Konishi, H., Yokoya, A., Shiwaku, H., Motohashi, H., Makita, T., Kashihara, Y., Hashimoto, S., Harami, T., Sasaki, T. A., Maeta, H., Ohno, H., Maezawa, H., Asaoka, S., Kanaya, H., Ito, K., Usami, N. & Kobayashi, K. (1996). *Nucl. Instrum. Methods*, A**372**, 322–332.
Kraft, S., Stümpel, J., Becker, P. & Kuetgens, U. (1996). *Rev. Sci. Instrum.* **67**, 681–687.
Krause, M. O. & Oliver, J. H. (1979). *J. Phys. Chem. Ref. Data*, **8**, 329.
Lai, B. & Cerrina, F. (1986). *Nucl. Instrum. Methods*, A**246**, 337–341.
Matz, W., Prokert, F., Schlenk, R., Claußner, J., Schell, N., Eichhorn, F. & Bernhard, G. (1996). *The Rossendorf Beamline at the ESRF (Project ROBL).* Internal report FZR-158. Forschungszentrum Rossendorf, Postfach 51 01 19, D-01314 Dresden, Germany.
Nitsche, H., Reich, T., Hennig, C., Roßberg, A., Geipel, G., Denecke, M. A., Baraniak, L., Panak, P., Abraham, A., Mack, B., Selenska-Pobell, S. & Bernhard, G. (1999). *Speciation, Techniques and Facilities for Radioactive Materials at Synchrotron Light Source: Workshop Proceedings*, Grenoble, France, 4–6 October 1998, pp. 15–27. Paris: OECD/NEA.
Pauschinger, D., Becker, K. & Ludewig, R. (1995). *Rev. Sci. Instrum.* **66**, 2177–2179.
Petiau, J., Calas, G., Petitmaire, D., Bianconi, A., Benfatto, M. & Marcelli, A. (1986). *Phys. Rev. B*, **34**, 7350–7361.
Petit-Maire, D., Petiau, J., Calas, G. & Jacquet-Francillon, N. (1989). *Physica B*, **158**, 56–57.
Swislow, G. (1996). *SPEC. X-ray Diffraction Software.* Certified Scientific Software, POB 390640, Cambridge, MA 01239, USA.
Thiele, E., Hecker, M. & Schell, N. (1999). *Mater. Sci. Forum.* In the press.
Yaita, T., Narita, H., Suzuki, S., Tachimori, S., Shiwaku, H. & Motohashi, H. (1998). *J. Alloy. Compd.* **271**, 184–188.
Yokoya, A., Sekiguchi, T., Saitoh, Y., Okane, T., Nakatani, T., Shimada, T., Kobayashi, H., Takao, M., Teraoka, Y., Hayashi, Y., Sasaki, S., Miyahara, Y., Harami, T. & Sasaki, T. A. (1998). *J. Synchrotron Rad.* **5**, 10–16.